AN ANALYTICAL APPROACH TO DESIGNING FRICTION DAMPERS IN TURBOMACHINERY BLADING

Josef Panovsky[1], Analytical Engineer

David G. Hendley, Staff Design Engineer

Raymond A. MacKay, Senior Staff Aeromechanical Engineer

GE Aircraft Engines
Cincinnati, Ohio and Lynn, Massachusetts

ABSTRACT

Aircraft engine turbomachinery blading operates in an environment that induces vibration which can lead to failure through high–cycle fatigue. This vibration can often be reduced to acceptable levels by friction dampers, which dissipate energy by capitalizing on the resulting relative motion between the blade and a motionless structure or adjacent vibrating blades. The key to optimizing a given damper design is to determine the dynamic weight at which the maximum energy is dissipated without locking the blade at the damper contact point. As the design of turbomachinery blading progresses towards higher–loaded stages with more complex geometry, vibratory modes beyond the primary beam bending become more prominent. This paper will discuss the development of an analytical method to predict damper effectiveness for any blade mode. The analysis is based on a component mode method, and includes provisions for modeling stick–slip at the friction contact. Multiple damper contact points can be evaluated, and the damper design can be blade–to–ground or blade–to–blade with arbitrary phase angle. The results of a series of lab tests with simple beam specimens to evaluate the principal damper design variables will be presented along with the corresponding analytical predictions.

1. GE Aircraft Engines, 1 Neumann Way, M/D A334, Cincinnati, Ohio 45215. Tel (513) 583–5117.

1 INTRODUCTION

Dampers for turbomachinery blading have traditionally been designed through the use of experience and lab testing. Until recently, there was little analytical support available because of the complexity of the governing equations, which are nonlinear due to the friction forces present at the blade–damper contact points. The solution is also complicated by the requirement to know all three spatial components of the relative motion at these contact points. Recent development efforts, however, have resulted in analytical methods which can be used to evaluate the effectiveness of the damper in reducing blade vibration.

There are certain basic characteristics that qualitatively describe the effects of a damper on the vibratory motion of a blade. The most important characteristic is the existence of an optimal friction force for a given excitation. As the damper weight is varied, a value can be found which minimizes the blade response, and increasing or decreasing the damper weight from this value will cause the vibratory response of the blade to increase. Variables such as shank–to–airfoil stiffness ratio can modify this optimum weight. A damper also causes the vibratory mode shape to change, and in the extreme a very heavy damper can reduce the relative motion to a point that the airfoil is vibrating alone without any mechanical damping. As a result of the damper and the mode shape change, the resonant frequency will increase, and this change may be quite significant in some cases. An example of a blade and damper along with the nomenclature that will be used in this paper is shown in Figure 1.

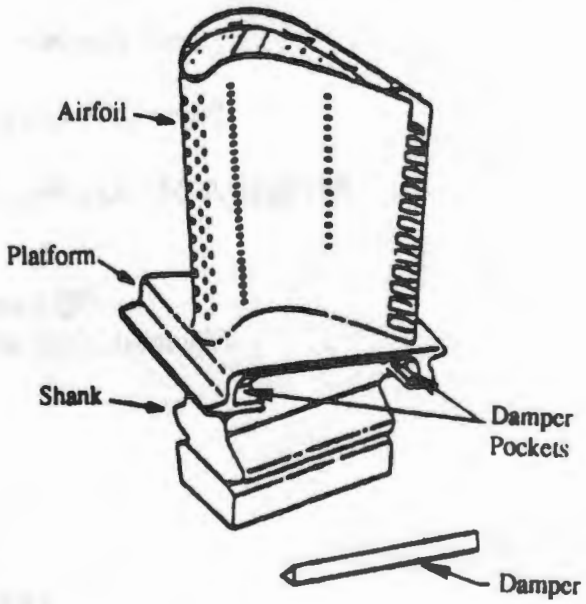

Figure 1. Typical turbine blade with self–centering damper. The damper rides under the platform and contacts adjacent blades.

The method outlined here follows from references [1] through [5]. The main emphasis of this paper is the extension of these methods to efficiently analyze self–centering blade–to–blade dampers, which are carried between the platforms of adjacent blades. Engine rotation causes the centrifugal forces which load the dampers against the blades, and the design of the dampers is such that they always remain in contact with each adjacent blade, hence the term "self–centering". To begin, though, blade–to–ground dampers are considered to introduce the methodology which will be used.

2 ANALYTICAL APPROACH

2.1 BLADE–TO–GROUND DAMPERS. Because of the complexity of the geometry of turbomachinery blades, a detailed model such as a three–dimensional finite element analysis is required to accurately assess the natural frequencies and their associated mode shapes. Since frequency analysis is nearly always done as a part of the blade design process, it is assumed that such a model exists

and the governing equations will be used as a starting point. The equations of motion for the blade are then

$$[m]\{\ddot{u}\} + [c]\{\dot{u}\} + [k]\{u\} = \{P\} - \{F\} \tag{1}$$

where

u = displacement of each degree of freedom
m = mass matrix
c = viscous damping matrix (assumed proportional)
k = stiffness matrix
P = driving force
F = friction force.

For typical turbine blade models, (1) represents a very large set of equations, which are all coupled through the mass, stiffness, and damping matrices. While P will be specified, the F are nonlinear functions, so the equations cannot be solved directly. One approach to dealing with this set of equations is to turn to a modal method, where it is assumed that the natural frequencies and mode shapes have been previously determined by solving the eigenvalue problem,

$$[m]\{\ddot{u}\} + [k]\{u\} = \{0\} \ . \tag{2}$$

An important mathematical property of the mode shapes is that they form an orthogonal set, which is relevant because the mode shapes can then be used as coordinates to describe the motion. The physical displacements can be represented as a superposition of the mode shapes,

$$\{u\} = [\Phi]\{q\} \tag{3}$$

where

Φ = matrix of mode shapes, ϕ_i
q = modal amplitudes.

Note that the physical displacements are a function of position and time, while the mode shapes are a function of position only and the modal amplitudes are a function of time only. This can be substituted into (1), and after pre–multiplying by the transpose of $[\Phi]$,

$$M_i[\ddot{q}_i + 2\zeta_i\omega_i\dot{q}_i + \omega_i^2 q_i] = Pp_i - Fa_i \tag{4}$$

where

M_i = modal mass of i^{th} mode
ω_i = natural frequency
ζ_i = viscous damping
p_i = mode shape component at the location of the excitation force for the i^{th} mode
a_i = mode shape component at the location of the friction damper for the i^{th} mode.

The mass, stiffness, and damping matrices have been diagonalized due to the orthogonality of the modes, meaning the left–hand sides of (4) are completely de–coupled. Any physical quantity can be described in terms of the modal amplitudes by using (3), and in particular, the physical displacement at the damper contact is given by

$$\xi = \sum_{i=1}^{n} a_i q_i \ . \tag{5}$$

The equations of motion will be simplified through the use of the method of harmonic balance. The displacements and forces are assumed to be of the form

$$\begin{aligned} q_i &= q_i^c \cos \Omega t + q_i^s \sin \Omega t \\ P &= P^c \cos \Omega t + P^s \sin \Omega t \\ F &= F^c \cos \Omega t + F^s \sin \Omega t \\ \xi &= \xi^c \cos \Omega t + \xi^s \sin \Omega t \end{aligned} \tag{6}$$

where Ω is the driving frequency. Note that the damper displacement, for example, can also be written in terms of its magnitude and phase,

$$\xi = \bar{\xi} \sin(\Omega t + \psi) \ . \tag{7}$$

By applying the harmonic balance method to (4), expressions for the modal amplitudes can be determined,

$$q_i^c = \frac{(P^c p_i - F^c a_i)(\omega_i^2 - \Omega^2) - (P^s p_i - F^s a_i)(2\zeta_i \omega_i \Omega)}{M_i[(\omega_i^2 - \Omega^2)^2 + (2\zeta_i \omega_i \Omega)^2]} \tag{8}$$

$$q_i^s = \frac{(P^c p_i - F^c a_i)(2\zeta_i \omega_i \Omega) + (P^s p_i - F^s a_i)(\omega_i^2 - \Omega^2)}{M_i[(\omega_i^2 - \Omega^2)^2 + (2\zeta_i \omega_i \Omega)^2]} \ .$$

Substituting these into (5), then using (6) and equating like terms,

$$\begin{aligned} \xi^c &= A1\ P^c - A2\ F^c - A3\ P^s + A4\ F^s \\ \xi^s &= A1\ P^s - A2\ F^s + A3\ P^c - A4\ F^c \end{aligned} \tag{9}$$

where

$$A1 = \sum_{i=1}^{n} \frac{p_i a_i (\omega_i^2 - \Omega^2)}{\gamma_i} \qquad A3 = \sum_{i=1}^{n} \frac{p_i a_i (2\zeta_i \omega_i \Omega)}{\gamma_i}$$

$$A2 = \sum_{i=1}^{n} \frac{a_i a_i (\omega_i^2 - \Omega^2)}{\gamma_i} \qquad A4 = \sum_{i=1}^{n} \frac{a_i a_i (2\zeta_i \omega_i \Omega)}{\gamma_i}$$

and

$$\gamma_i = M_i[(\omega_i^2 - \Omega^2)^2 + (2\zeta_i \omega_i \Omega)^2] \ .$$

Following [2], the damper is taken to be a Coulomb friction element and a spring in series, so that slip occurs in the friction element when the spring force reaches a value of μN. Lab measurements have shown this to be a good idealization of the behavior of the damper. The damper displacement and the resulting friction force are defined in Figure 2, and it is noted that the displacement can be written

$$\xi = \bar{\xi} \cos \theta \tag{10}$$

and the start of slip in the half-cycle $0<\theta<\pi$ can be determined to be

$$\Theta = \cos^{-1} \left(1 - \frac{2\mu N}{k\bar{\xi}}\right) \ . \tag{11}$$

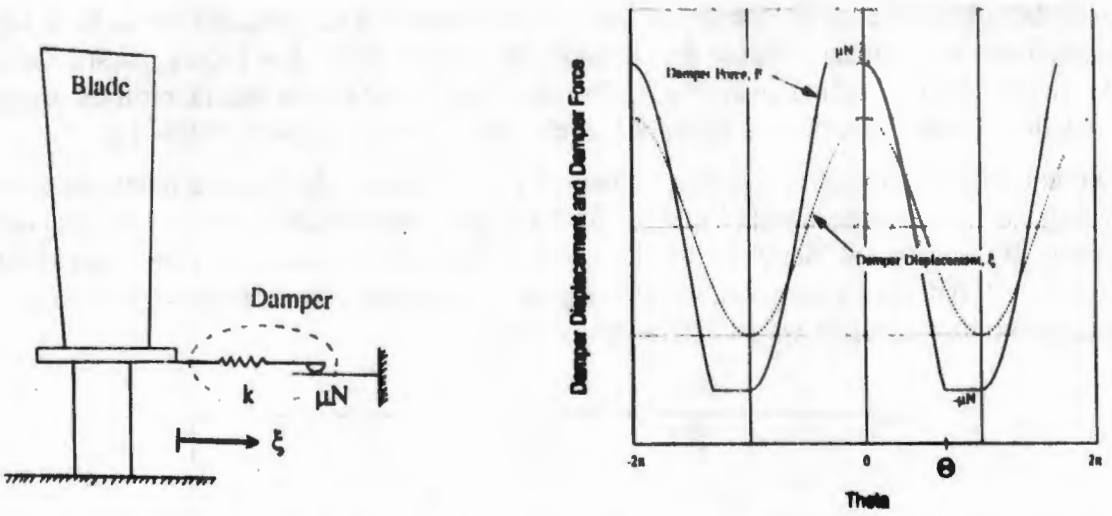

Figure 2. Behavior of friction interface. The friction element, shown schematically with the blade, behaves as a spring until the slip value is attained.

The damper force is expanded in a Fourier series and truncated after the fundamental harmonic terms, resulting in

$$F = G1\,\bar{\xi}\cos\theta + G2\,\bar{\xi}\sin\theta \tag{12}$$

where

$$G1 = \frac{k}{\pi}(\Theta - \frac{1}{2}\sin 2\Theta)$$

$$G2 = -\frac{k}{\pi}\sin^2\Theta \ .$$

Comparing (6), (7), and (10), this equation becomes

$$\begin{aligned} F^c &= G1\,\xi^c - G2\,\xi^s \\ F^s &= G1\,\xi^s + G2\,\xi^c \ . \end{aligned} \tag{13}$$

This is substituted into (9), which is rearranged to give

$$\begin{aligned} E1 &= -D1\,\xi^c + D2\,\xi^s \\ E2 &= D1\,\xi^s + D2\,\xi^c \end{aligned} \tag{14}$$

where

$$D1 = 1 + A2\,G1 - A4\,G2 \qquad E1 = A1\,P^c - A3\,P^s$$

$$D2 = A2\,G2 + A4\,G1 \qquad E2 = A1\,P^s + A3\,P^c \ .$$

Equation (14) can be solved to give

$$\bar{\xi} = \sqrt{\frac{E1^2 + E2^2}{D1^2 + D2^2}} \tag{15}$$

$$\tan\psi = \frac{D1\,E1 + D2\,E2}{D1\,E2 - D2\,E1} \ .$$

Because $D1$ and $D2$ are transcendental functions of Θ, iteration is required to solve (15). A simple bisection method is utilized because Θ is bounded by $0<\Theta<\pi$. Once ξ is known, substitution into (13) gives all the forces acting on the blade. The modal amplitudes q_i are then determined using (8), and any physical displacement or stress of interest can then be obtained by following (3).

A common approach to assess the effectiveness of a given damper design is to repeat the solution for a range of driving frequencies, determining the displacement and/or stress at key locations on the blade. By varying the friction or driving forces, a parametric study can be conducted as shown in Figure 3. From this information, which includes the resonant stress, frequency, and log decrement, the optimum damper weight can be determined.

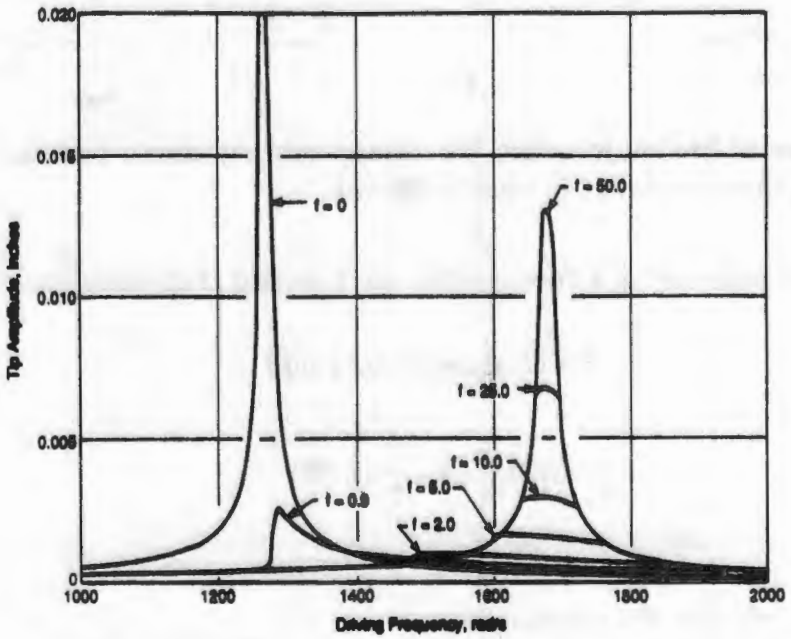

Figure 3. Frequency response for various friction forces. By using a series of driving frequencies, the maximum response for a given friction force can be found.

2.2 BLADE–TO–BLADE DAMPERS. A common design approach for blade dampers is to place the damper between two blades, so that centrifugal forces cause the damper to remain in contact with the platform of each blade as they vibrate. Because of the free–floating nature of the damper, its relative motion along each face of the blade platform must be determined. Simply knowing the absolute motion of the damper is not sufficient. It is assumed that these vibratory motions are small enough so that the scrubbing surfaces move in translation only, that the centrifugal force will cause the damper to move radially outward as far as the platforms allow, and this motion will be continuous sliding. These assumptions are consistent with good damper design practices.

The damper is shown schematically in Figure 4. With the assumptions made for damper motion, the damper position is known once the motions of the two blades have been specified. Motion out of this plane is considered separately because its effect on damping depends on the physical damper restraints, and in addition, this component is usually not a source of reliable damping. If an oblique coordinate system is placed along the contact surfaces as shown, with the origin at the damper apex, determination of the relative motion becomes much easier. The transformation equations to obtain

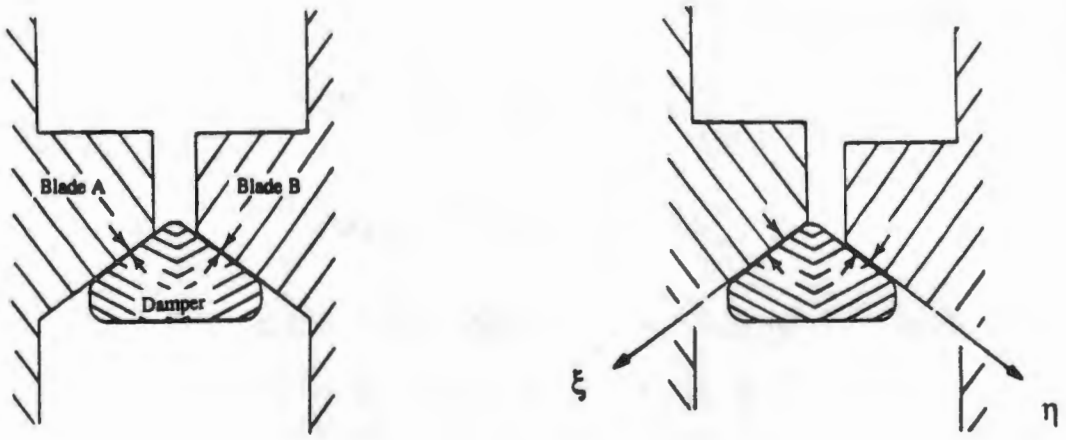

Figure 4. Blade–to–Blade Damper. The motion of the damper is shown schematically. Note that the location of the damper is determined by the location of the contact points on the blades.

the vibratory motions in terms of the oblique coordinates from the usual Cartesian reference frame can be found in [8]. Because rotations of the blade contact surfaces are ignored, the A–blade damper surface will move along lines parallel to ξ, while the B–blade moves parallel to η. The absolute damper motion is seen to correspond to the ξ–motion of B and the η–motion of A, and the relative motion along each face of the damper is given directly by

$$\begin{aligned} \xi &= \xi^B_{abs} - \xi^A_{abs} \\ \eta &= \eta^B_{abs} - \eta^A_{abs} \,. \end{aligned} \tag{16}$$

In this equation, the "abs" subscript indicates absolute components of motion while the lack of a subscript indicates a relative term. For clarity, the discussion will be limited to motion in the ξ direction; similar results would be applicable to the η component. Replacing the blade displacement in (16) with the modal components,

$$\xi = \sum_{i=1}^{n} a_i q_i^A - \sum_{i=1}^{n} b_i q_i^B \tag{17}$$

where

a_i = mode shape in the ξ direction for the i^{th} mode at the damper contact of blade A

q_i^A = modal amplitude of blade A

b_i = mode shape in the ξ direction for the i^{th} mode at the damper contact of blade B

q_i^B = modal amplitude of blade B.

Now assume that blades A and B have identical responses with the exception of an interblade phase angle, Φ. Again assuming harmonic motion, the modal amplitude can be written

$$\begin{aligned} q_i^A &= q_i^c \cos \Omega t + q_i^s \sin \Omega t \\ q_i^B &= q_i^c \cos(\Omega t + \Phi) + q_i^s \sin(\Omega t + \Phi) \end{aligned} \tag{18}$$

where the cosine and sine terms on the right–hand side of both equations refer to blade A.

Expanding and substituting into (17),

$$\xi^c = \sum_{i=1}^{n}(a_i - b_i\cos\Phi)q_i^c - \sum_{i=1}^{n}(b_i\sin\Phi)q_i^s \qquad (19)$$

$$\xi^s = \sum_{i=1}^{n}(a_i - b_i\cos\Phi)q_i^s + \sum_{i=1}^{n}(b_i\sin\Phi)q_i^c \ .$$

The relations given by (8) still apply, and substituting into (19) leads to

$$\begin{aligned} \xi^c &= C1\,P^c - C2\,F^c - C3\,P^s + C4\,F^s \\ \xi^s &= C1\,P^s - C2\,F^s + C3\,P^c - C4\,F^c \end{aligned} \qquad (20)$$

where

$$\begin{aligned} C1 &= A1 - B1\cos\Phi - B3\sin\Phi \\ C2 &= A2 - B2\cos\Phi - B4\sin\Phi \\ C3 &= A3 - B3\cos\Phi + B1\sin\Phi \\ C4 &= A4 - B4\cos\Phi + B2\sin\Phi \end{aligned}$$

and

$$B1 = \sum_{i=1}^{n}\frac{p_i b_i(\omega_i^2 - \Omega^2)}{\gamma_i} \qquad B3 = \sum_{i=1}^{n}\frac{p_i b_i(2\zeta_i\omega_i\Omega)}{\gamma_i}$$

$$B2 = \sum_{i=1}^{n}\frac{a_i b_i(\omega_i^2 - \Omega^2)}{\gamma_i} \qquad B4 = \sum_{i=1}^{n}\frac{a_i b_i(2\zeta_i\omega_i\Omega)}{\gamma_i} \ .$$

The forces contributed by the damper are still given by (12), where it is understood that ξ is the motion of the blade relative to the damper at the contact point. Then (20) is identical in form to (9), the only difference in the equations being in the C–coefficients. In fact, (9) can be obtained by taking the b_i to be zero. The solution can then proceed in a manner identical to the blade–to–ground damper, iterating on (15) to find the relative displacement.

2.3 MULTIPLE DAMPERS. The analysis is now extended to the case of multiple damper locations with multiple excitation forces. Because the blade–to–blade analysis will easily degenerate to the blade–to–ground case, only these results are derived here. Also, because the approach taken is identical to that for a single damper, detail will be kept to a minimum.

The equations of motion are generalized to

$$M_i[\ddot{q}_i + 2\zeta_i\omega_i\dot{q}_i + \omega_i^2 q_i] = \sum_l P_l\,p_{li} - \sum_j F_j\,a_{ji} \qquad (21)$$

where

P_l = excitation force at l^{th} location
p_{li} = mode shape component at the l^{th} location for the i^{th} mode
F_j = friction force at the j^{th} damper location
a_{ji} = mode shape component at the j^{th} damper for the i^{th} mode for blade A.

The relative motion at the j^{th} damper, obtained by starting with (17), assuming harmonic motion,

and substituting for the $q_{i,}$ is given by

$$\xi_j^c = \sum_l C1_{jl} P_l^c - \sum_J C2_{jJ} F_J^s - \sum_l C3_{jl} P_l^s + \sum_J C4_{jJ} F_J^c$$
$$\xi_j^s = \sum_l C1_{jl} P_l^s - \sum_J C2_{jJ} F_J^s + \sum_l C3_{jl} P_l^c - \sum_J C4_{jJ} F_J^c \qquad (22)$$

where

$$C1_{jl} = A1_{jl} - B1_{jl}\cos\Phi - B3_{jl}\sin\Phi$$
$$C2_{jJ} = A2_{jJ} - B2_{jJ}\cos\Phi - B4_{jJ}\sin\Phi$$
$$C3_{jl} = A3_{jl} - B3_{jl}\cos\Phi + B1_{jl}\sin\Phi$$
$$C4_{jJ} = A4_{jJ} - B4_{jJ}\cos\Phi + B2_{jJ}\sin\Phi$$

and

$$A1_{jl} = \sum_{i=1}^{n} \frac{a_{ji} p_{li} (\omega_i^2 - \Omega^2)}{\gamma_i} \qquad B1_{jl} = \sum_{i=1}^{n} \frac{b_{ji} p_{li} (\omega_i^2 - \Omega^2)}{\gamma_i}$$
$$A2_{jJ} = \sum_{i=1}^{n} \frac{a_{ji} a_{Ji} (\omega_i^2 - \Omega^2)}{\gamma_i} \qquad B2_{jJ} = \sum_{i=1}^{n} \frac{b_{ji} a_{Ji} (\omega_i^2 - \Omega^2)}{\gamma_i}$$
$$A3_{jl} = \sum_{i=1}^{n} \frac{a_{ji} p_{li} (2\zeta_i \omega_i \Omega)}{\gamma_i} \qquad B3_{jl} = \sum_{i=1}^{n} \frac{b_{ji} p_{li} (2\zeta_i \omega_i \Omega)}{\gamma_i}$$
$$A4_{jJ} = \sum_{i=1}^{n} \frac{a_{ji} a_{Ji} (2\zeta_i \omega_i \Omega)}{\gamma_i} \qquad B4_{jJ} = \sum_{i=1}^{n} \frac{b_{ji} a_{Ji} (2\zeta_i \omega_i \Omega)}{\gamma_i} .$$

Because the force at each damper is only a function of the relative motion at that location, (12) still applies for each damper, and (22) becomes

$$E1_j = \sum_J D1_{jJ} \xi_J^c - \sum_J D2_{jJ} \xi_J^s$$
$$E2_j = \sum_J D1_{jJ} \xi_J^s + \sum_J D2_{jJ} \xi_J^c \qquad (23)$$

where

$$D1_{jJ} = \delta_{jJ} + \sum_J C2_{jJ} G1_J - \sum_J C4_{jJ} G2_J \qquad E1_j = \sum_l (C1_{jl} P_l^c - C3_{jl} P_l^s)$$
$$D2_{jJ} = \sum_J C2_{jJ} G2_J + \sum_J C4_{jJ} G1_J \qquad E2_j = \sum_l (C1_{jl} P_l^s + C3_{jl} P_l^c)$$

where δ_{jJ} is defined to be the Kronecker delta. The displacements at the various dampers are coupled through the *D*–matrices so the result is a set of coupled, nonlinear algebraic equations, with one equation for each damper location and direction. The solution method employed for a single damper can no longer be used and is replaced by a method based on Newton–Raphson iteration. This algorithm, though, cannot guarantee convergence, and in practice assumptions are made to reduce the system to a single equivalent damper whenever possible.

3 EXPERIMENTAL VERIFICATION OF ANALYTICAL METHOD

Verification of the preceding analytical methods by laboratory experiments was deliberately planned to take place in several stages, beginning with a simple beam model and eventually leading to actual turbine blade geometry. This paper shows analytical comparisons with experimental re-

sults for simple beam models of various geometries. Specimens were constructed with a simulated airfoil, platform, and shank region as shown in Figure 5. A number of different specimen geometries were tested and the effects of the most significant variable, shank thickness, are illustrated for blade–to–ground, blade–to–blade, and multiple damper test configurations.

3.1 BLADE–TO–GROUND DAMPER. The first specimens were tested with a blade–to–ground arrangement as shown in Figure 5. This arrangement allowed the normal load on the damping surface to be varied and the resulting dynamic friction force to be measured. Excitation was provided by a shaker table. Strain gages were placed on the specimens to monitor the vibration as a result of the action of the bar damper.

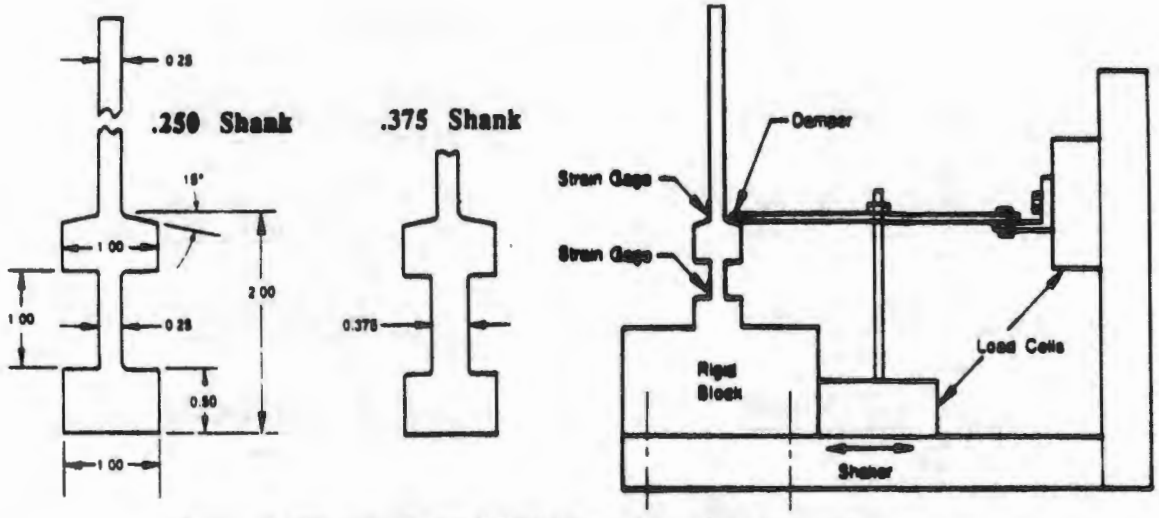

Figure 5. Simple Beam Model and Associated Test Apparatus.

The vibratory response of the simple beam model in terms of airfoil root stress versus damper load is shown in Figure 6. The effect on the first flexural (primary) frequency with increasing damper load is also shown. Each set of data for the two different shank thicknesses shows very good correlation to the analytical method.

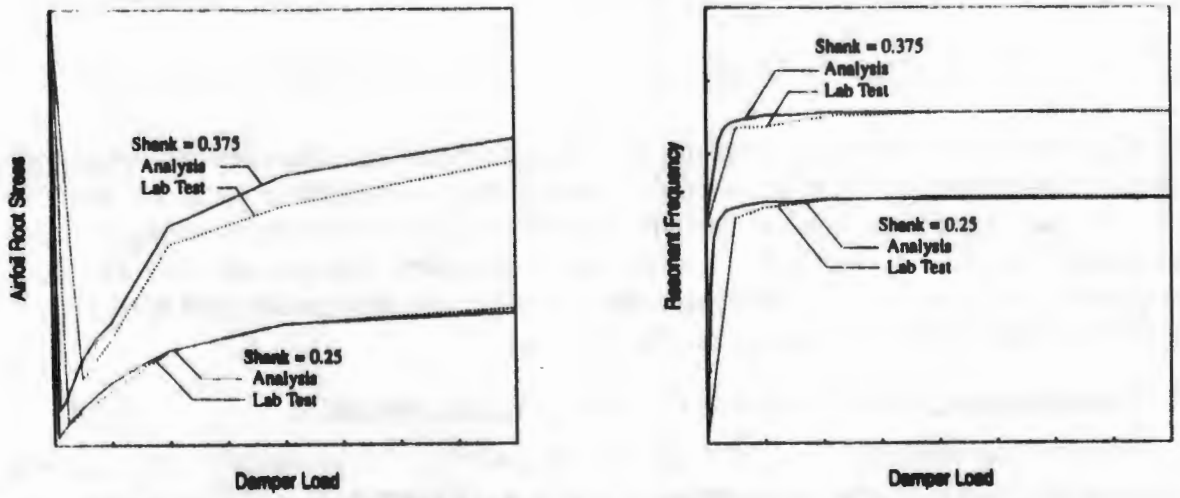

Figure 6. Comparison of Analytical Method with Test Data for Blade–to–Ground Damper.

3.2 BLADE–TO–BLADE DAMPER. Testing of a blade–to–blade configuration was conducted using the apparatus shown in Figure 7. Two identical simple beam models were clamped in a fixture with a damper supported between adjacent platforms and loaded by means of a wire attached to a pulley. The damper load was varied over a wide range by applying varying tensile loads in the wire. Excitation was provided by means of a pulsing air jet (siren), exciting the specimens in the first flexural mode of vibration. The level of excitation was controlled by the air jet supply pressure, and the frequency was controlled by the speed of the air jet rotor.

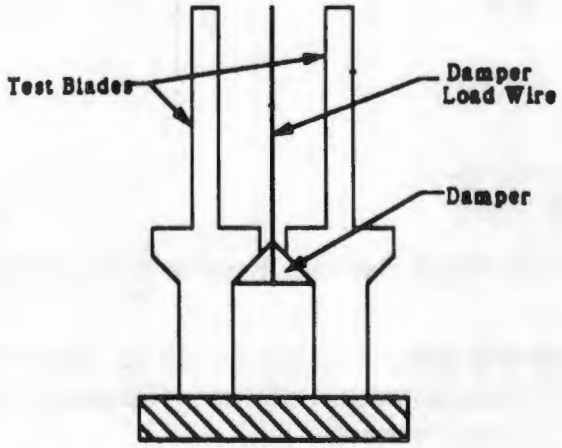

Figure 7. Blade–to–Blade Damper Test Apparatus.

Vibratory stresses were measured at the airfoil root, the top of the blade shank, and at the bottom of the blade shank. Two different levels of excitation were used, and results were obtained for in–phase and out–of–phase blade motions.

Results for the in–phase and out–of–phase damper tests are shown in Figures 8 and 9, respectively. The averages of several experimental data sets are shown and compared with analytical predictions. Airfoil root stress at the two levels of excitation and resonant frequency predictions at the lower level are given.

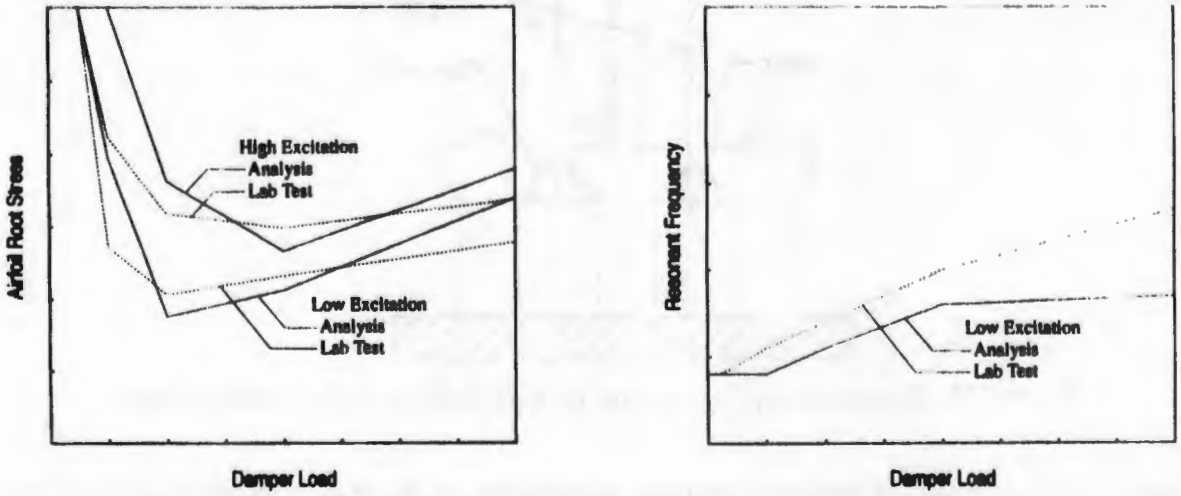

Figure 8. Blade–to–Blade Damping Results: In–Phase Vibration.

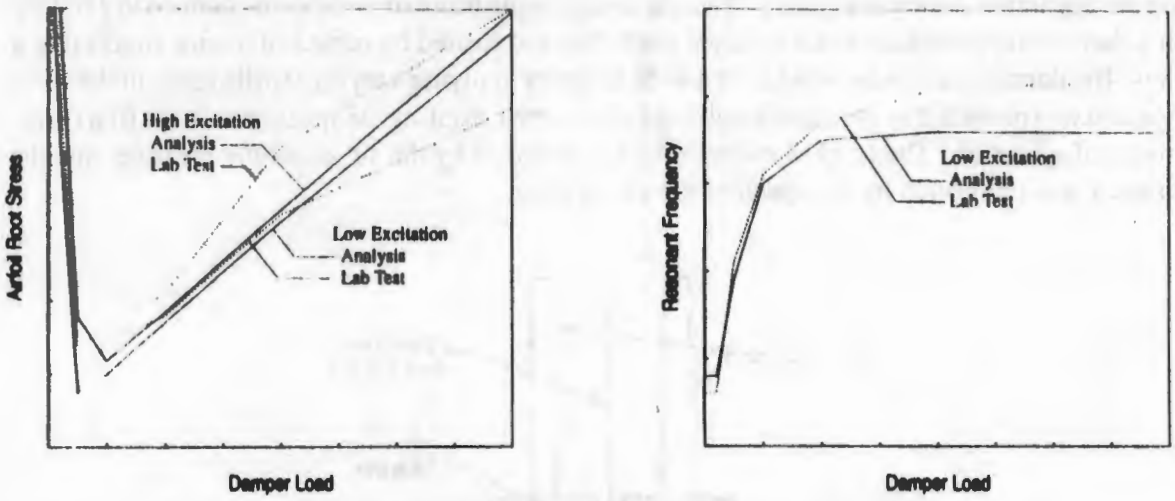

Figure 9. Blade–to–Blade Damping Results: Out–of–Phase Vibration.

The analytical predictions for both levels of excitation show good agreement with the experimental data for in–phase and out–of–phase vibration. Prediction of frequency change as a result of increasing damper load also shows good agreement.

3.3 TYPICAL DAMPER EFFECTIVENESS TEST. The final stage of experimental testing was designed to duplicate a typical set–up used in the laboratory to conduct damper effectiveness testing on actual engine hardware. The testing on model blades was conducted using a damper positioned either side of a test blade with the dampers retained by two additional blades with airfoils removed, as shown in Figure 10. The test blade was excited by means of the air siren, but the "dummy" blades do not vibrate because of the removal of their airfoil. Again several variables were examined, and the tests were repeated to obtain an average for each setting.

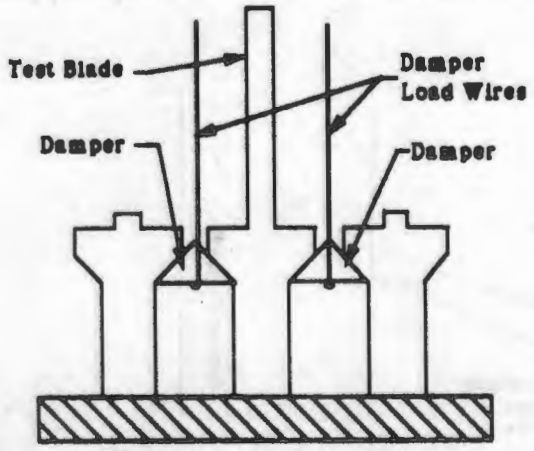

Figure 10. Experimental Set–up for Typical Damper Effectiveness Test.

Figure 11 shows the airfoil root stress and resonant frequency change plotted against damper load for three shank thicknesses compared to analytical results. There is good agreement between the

analytical results and the experimental data. This again supports the use of this analytical technique to predict the optimum damper weight to ensure maximum damper effectiveness.

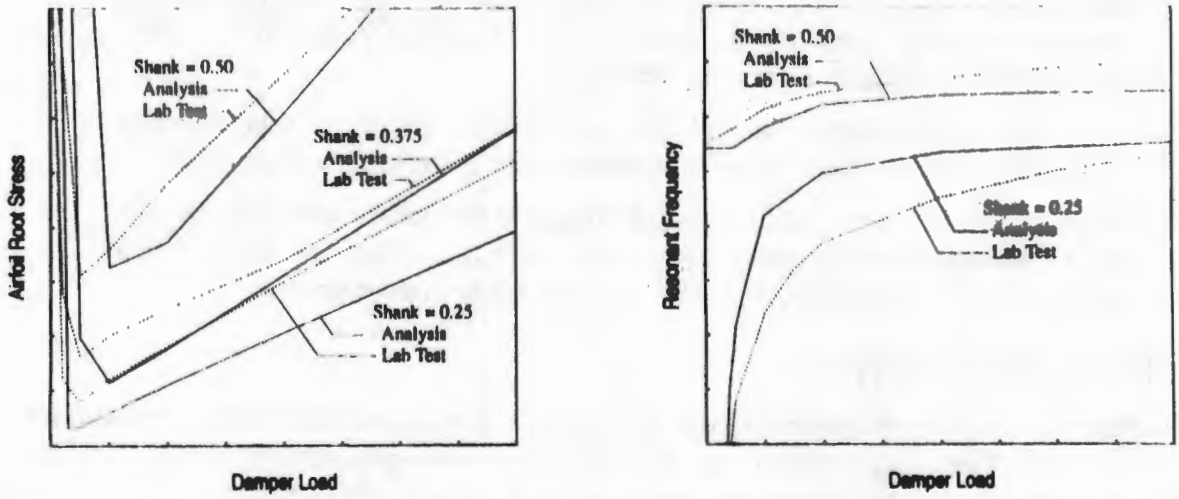

Figure 11. Comparison of Analytical Method with Test Data for Damper Effectiveness Test.

4 DISCUSSION OF RESULTS

A full range of experimental testing has been carried out examining variables such as damper–to–platform contact angle, platform width, and shank thickness. Various excitation levels were used, and results were plotted for an average of each data set. It was decided to present the results for the variation in shank thickness because these illustrated the most pronounced effect on blade damping, and it has been demonstrated within this paper that the analytical method was able to predict the results for this variable accurately. Predictions for other variables were also good although not shown here for brevity. It should be noted that, while comparison of the analytical method with experimental results has been presented for only the primary bending mode, the method is capable of predicting the damper effectiveness for any mode of interest.

The analytical method is able to determine the "optimum" damper weight by predicting the actual decrease and increase in vibratory response as the damper load is increased. The optimum theoretical weight of the damper is that weight which, when converted into an equivalent load at engine speed, produces the minimum vibratory response.

A damper can increase the frequency of the blade by significantly high percentages. For first flexural modes this can be as large as 25% for a cooled turbine blade. It is, therefore, important to be able to predict this increase accurately as it has a pronounced significance when considering resonances with stimuli that could produce detrimental responses of the blades. The analysis has demonstrated its ability to predict this frequency increase accurately for the test cases presented and offers a means of correcting for damping effects when assessing resonances in engines.

The analysis was able to predict the point at which the damper load becomes so high that it prevents motion in the shank and causes the airfoil to vibrate in an undamped mode. This condition is potentially dangerous for the airfoil because of the high vibratory stresses involved.

5 CONCLUSIONS

- A new analytical method has been developed which enables a blade designer to pre–determine the effectiveness of a damper design prior to manufacture and bench test.
- The method is able to predict the optimum damper load for maximum effectiveness and the point at which the damper is so heavy that it effectively "locks–up" the airfoil at the platforms so that it is virtually undamped.
- Comparisons made between the analytical method and experimental data generated by using simple beam models confirms the accuracy of the tool for design use.
- Future work will be centered around developing this analytical method for use with actual cooled turbine blade geometry and applying it to a rotating system of blades to predict damped responses compared to engine blade strain gage data.

6 ACKNOWLEDGEMENTS

The authors wish to acknowledge the contributions of R.O. Brooks and V.C. Gallardo towards the development of this damping methodology. Appreciation is also expressed to A. Rotsko, J. Miller, L. Joyce, and W. Day for the experimental work and to others at GEAE who have supported this effort.

REFERENCES

1. Dowell, E.H., "The Behavior of a Linear Damped Modal System with a Non–linear Spring–Mass–Dry Friction Damper System Attached," *Journal of Sound and Vibration*, Vol. 89, 1983, pp. 65–84.

2. Griffin, J.H., "Friction Damping of Resonant Stresses in Gas Turbine Engine Airfoils," ASME *Journal of Engineering for Power*, Vol. 102, Apr. 1980, pp. 329–333.

3. Menq, C.–H., and Griffin, J.H., "A Comparison of Transient and Steady State Finite Element Analyses of the Forced Response of a Frictionally Damped Beam," ASME *Journal of Vibration, Acoustics, Stress, and Reliability in Design*, Vol. 107, Jan. 1985, pp. 19–25.

4. Cameron, T.M., Griffin, J.H., Kielb, R., and Hoosac, T.M., "An Integrated Approach for Friction Damper Design," ASME Bound Volume DE–5, Sept. 1987, pp. 205–212.

5. Tongue, B.H., and Dowell, E.H., "Component Mode Analysis of Nonlinear, Nonconservative Systems," ASME *Journal of Applied Mechanics*, Vol. 50, Mar. 1983, pp. 204–209.

6. den Hartog, J.P., "Forced Vibrations with Combined Coulomb and Viscous Friction," *Trans ASME*, Paper APM–53–9, 1931, pp.107–115.

7. Goodman, L.E. and Klumpp, J.H., "Analysis of Slip Damping With Reference to Turbine Blade Vibration," ASME *Journal of Applied Mechanics*, Sept. 1956, pp. 421–429.

8. Arfken, G., *Mathematical Methods for Physicists*, 2nd ed., Academic Press, New York, 1970.